Hyperpolarized ^{129}Xe MRI and Spectroscopy of Gas-Exchange Abnormalities in Nonspecific Interstitial Pneumonia

*David G. Mummy, PhD • Elianna A. Bier, MS • Ziyi Wang, PhD • Jennifer Korzekwinski, RT (N), CNMT •
Lake Morrison, MD • Christina Barkauskas, MD • H. Page McAdams, MD • Robert M. Tighe, MD •
Bastiaan Driehuys, PhD • Joseph G. Mammarappallil, MD, PhD*

From the Department of Radiology (D.G.M., J.K., B.D., J.G.M.), Center for In Vivo Microscopy (D.G.M., B.D.), Department of Biomedical Engineering (E.A.B., Z.W., B.D.), Department of Medicine (L.M., C.B., H.P.M., R.T.), and Department of Medical Physics (B.D.), Duke University, DUMC Box 3302, Durham, NC 27710. Received October 27, 2020; revision requested January 11, 2021; revision received May 12; accepted May 21. **Address correspondence to** J.G.M. (e-mail: *joseph.mammarappallil@duke.edu*).

Background: Recent studies demonstrate that antifibrotic drugs previously reserved for idiopathic pulmonary fibrosis (IPF) may slow progression in other interstitial lung diseases (ILDs), creating an urgent need for tools that can sensitively assess disease activity, progression, and therapy response across ILDs. Hyperpolarized xenon 129 (^{129}Xe) MRI and spectroscopy have provided noninvasive measurements of regional gas-exchange abnormalities in IPF.

Purpose: To assess gas exchange function using ^{129}Xe MRI in a group of study participants with nonspecific interstitial pneumonia (NSIP) compared with healthy control participants.

Materials and Methods: In this prospective study, participants with NSIP and healthy control participants were enrolled between November 2017 and February 2020 and underwent ^{129}Xe MRI and spectroscopy. Quantitative imaging provided three-dimensional maps of ventilation, interstitial barrier uptake, and transfer into the red blood cell (RBC) compartment. Spectroscopy provided parameters of the static RBC and barrier uptake compartments, as well as cardiogenic oscillations in RBC signal amplitude and chemical shift. Differences between NSIP and healthy control participants were assessed using the Wilcoxon rank-sum test.

Results: Thirty-six participants with NSIP (mean age, 57 years ± 11 [standard deviation]; 27 women) and 15 healthy control participants (mean age, 39 years ± 18; two women) were evaluated. Participants with NSIP had no difference in ventilation compared with healthy control participants (median, 4.4% [first quartile, 1.5%; third quartile, 8.7%] vs 6.0% [first quartile, 2.8%; third quartile, 6.9%]; *P* = .91), but they had a higher barrier uptake (median, 6.2% [first quartile, 1.8%; third quartile, 23.9%] vs 0.53% [first quartile, 0.33%; third quartile, 2.9%]; *P* = .003) and an increased RBC transfer defect (median, 20.6% [first quartile, 11.6%; third quartile, 27.8%] vs 2.8% [first quartile, 2.3%; third quartile, 4.9%]; *P* < .001). NSIP participants also had a reduced ratio of RBC-to-barrier peaks (median, 0.24 [first quartile, 0.19; third quartile, 0.31] vs 0.57 [first quartile, 0.52; third quartile, 0.67]; *P* < .001) and a reduced RBC chemical shift (median, 217.5 ppm [first quartile, 217.0 ppm; third quartile, 218.0 ppm] vs 218.2 ppm [first quartile, 217.9 ppm; third quartile, 218.6 ppm]; *P* = .001).

Conclusion: Participants with nonspecific interstitial pneumonia had increased barrier uptake and decreased red blood cell (RBC) transfer compared with healthy controls measured using xenon 129 gas-exchange MRI and reduced RBC-to-barrier ratio and RBC chemical shift measured using spectroscopy.

©RSNA, 2021

Online supplemental material is available for this article.

Interstitial lung diseases (ILDs) share many clinical, genetic, and biologic features but can display widely variable progression, often resulting in irreversible scarring of the lung parenchyma (1). Idiopathic pulmonary fibrosis (IPF) is the most common and most lethal ILD, the prototype of progressive fibrotic lung disease. However, this is not the only type of ILD. Despite generally being considered less lethal than IPF, other ILDs, such as nonspecific interstitial pneumonia (NSIP), are also associated with substantial morbidity and mortality (2). An NSIP radiographic pattern is observed when there is

evidence of diffuse ground-glass opacities with reticulation that spares the immediate pleural space (3,4). NSIP is often seen in patients with an underlying diagnosis of a collagen vascular disease, but it can also be observed in cases without a clear association to autoimmunity (5). Historically, separating NSIP from IPF has been important, as NSIP has been more responsive to immunosuppression, which is largely avoided in IPF. However, it is becoming increasingly clear that progressive subtypes of non-IPF ILDs can have similar morbid outcomes to IPF (6,7), which raises the possibility of common

Abbreviations

H95% = observed 95th-percentile value in healthy control participants, ILD = interstitial lung disease, IPF = idiopathic pulmonary fibrosis, NSIP = nonspecific interstitial pneumonia, RBC = red blood cell, RDP = red blood cell defect percentage, VDP = ventilation defect percentage

Summary

Hyperpolarized xenon 129 MRI and spectroscopy are sensitive to abnormal interstitial barrier uptake and red blood cell transfer in participants with nonspecific interstitial pneumonia.

Key Results

- Thirty-six participants with nonspecific interstitial pneumonia (NSIP) who underwent xenon 129 MRI gas-exchange imaging had no difference in ventilation defect percentage compared with 15 healthy control participants (median, 4% vs 6.0%; $P = .91$).
- The same participants, however, had an increased high barrier uptake percentage (median, 6.2% vs 0.53%; $P = .003$) and an increased red blood cell transfer defect percentage (median, 20.6% vs 2.8%; $P < .001$).

mechanisms driving disease progression that could be evaluated using diagnosis-agnostic biomarkers.

IPF treatment in the United States was greatly advanced in 2014 after the U.S. Food and Drug Administration approval of pirfenidone and nintedanib, two antifibrotic drugs that considerably slowed disease progression (8,9). Although these drugs have generally been reserved for use in IPF, recent studies have provided compelling evidence that nintedanib is also effective in other progressive fibrotic lung diseases (10,11). Today, treatment efficacy is largely evaluated with relatively insensitive tools such as pulmonary function tests and 6-minute walk assessments. These measurements can characterize gross manifestations of fibrotic lung disease (6), but more refined methods are required to isolate and directly assess subtle biologic changes in pulmonary function, thereby improving clinical management of targeted ILD therapies.

Although CT is a diagnostic mainstay in ILDs, structural features observed therein are of limited value in assessing progression of fibrosis because they do not directly reflect lung function, which is correlated to disease progression (12). Further, the standard measures of lung function used in conventional pulmonary function testing cannot detect the regional differences in pathologic findings that are a hallmark of ILDs.

The use of MRI and spectroscopy with inhaled hyperpolarized xenon 129 (¹²⁹Xe) gas is rapid and well tolerated, and it enables regional assessment of pulmonary gas exchange (13). Inhaled ¹²⁹Xe diffuses from the alveoli into the alveolar-capillary interstitium (ie, interstitial barrier tissue) and then transiently binds with capillary red blood cells (RBCs) in the bloodstream (ie, RBC transfer) (14). The ¹²⁹Xe signals from each of these three compartments are resolved by means of distinct MR chemical shifts that allow them to be individually characterized with imaging (15) and with static and dynamic spectroscopy (14,16). ¹²⁹Xe MRI and spectroscopy studies in IPF have previously observed increases in barrier tissue uptake and decreased RBC transfer, as well as alterations in spectroscopic measures (16–20). However, understanding of ¹²⁹Xe MRI gas-exchange patterns in ILDs beyond IPF is lacking.

The purpose of our study was to characterize ¹²⁹Xe MRI and spectroscopy in patients with a diagnosis of NSIP, an ILD distinct from IPF, and to compare the results with measurements obtained in healthy control participants. We hypothesized that NSIP would be associated with significant gas-exchange abnormalities relative to our healthy control population.

Materials and Methods

Participant Recruitment and Characteristics

This prospective cross-sectional study was approved by the Duke institutional review board (approval no. Pro00025110) and was compliant with the Health Insurance Portability and Accountability Act. Hyperpolarized ¹²⁹Xe is treated as a drug by the U.S. Food and Drug Administration and is covered for this study under an investigational new drug approval (approval no. 109,490). Written informed consent was obtained from each participant before recruitment. Patients with a clinical and radiographic diagnosis of NSIP and healthy control participants were recruited consecutively and underwent ¹²⁹Xe MRI between 2017 and 2020. All participants were at least 18 years old and had no history of cardiac arrhythmia. Our NSIP population was derived from patients with a past diagnosis of NSIP by means of surgical pathologic results or CT with clinical collaboration and with concurrent provider appointments at our center during the study period. Patients recruited according to pathologic findings were excluded if they did not undergo CT. All participants underwent baseline pulmonary function tests to obtain forced vital capacity with spirometry and diffusing capacity of the lung for carbon monoxide with the single-breath method. CT scans were evaluated by cardiothoracic radiologists (J.G.M., with 7 years of experience, and H.P.M., with 30 years of experience) according to published criteria to confirm evidence of pulmonary fibrosis, absence of a usual interstitial pneumonia pattern, and no evidence of clinically significant air trapping (21). To identify participants likely to have an NSIP pathologic pattern, specific criteria included basilar-predominant findings of bronchiectasis and ground-glass opacity with subpleural sparing. CT was further used to assess pulmonary artery diameter measured on axial images at the level of its bifurcation, orthogonal to the long axis. Pulmonary function tests and demographic data gathered at the MRI visit were used to calculate an ILD–Gender-Age-Physiology score (22).

¹²⁹Xe Polarization and Dose Administration

¹²⁹Xe was hyperpolarized by means of continuous-flow spin-exchange optical pumping and cryogenic accumulation using commercially available hyperpolarized systems (Models 9820 and 9810, Polarean) and dispensed into a Tedlar dose delivery bag (Jensen Inert Products), as previously described (23). Hyperpolarized ¹²⁹Xe MRI and spectroscopy were performed with a 3.0-T scanner (Magnetom Trio, Siemens) during two separate breath holds of ¹²⁹Xe using a quadrature transmit-receive flexible vest coil (Clinical MR Solutions). Participants received a small dose for calibration and spectroscopy (target dose equivalent ≥50 mL; actual dose: mean, 63.6 mL ± 17.1 [standard deviation],
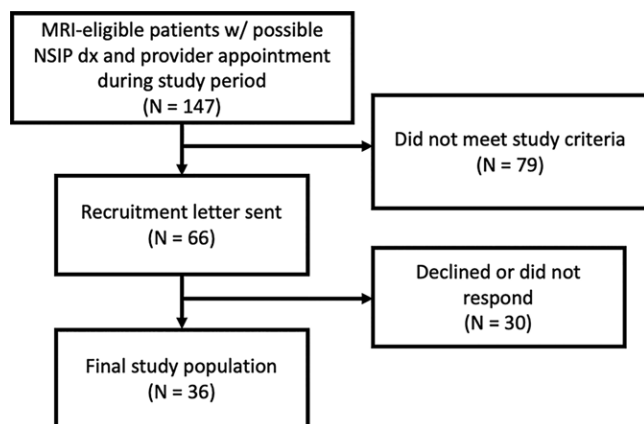
Figure 1: Flowchart of participant population. Our population with nonspecific interstitial pneumonia (NSIP) was derived from patients diagnosed with NSIP who had a provider appointment at our center between 2017 and 2020. Diagnosis (dx) was made by means of surgical pathologic findings or CT with clinical corroboration. Patients recruited according to pathologic results were excluded if they did not undergo CT, but patients diagnosed after undergoing CT were not required to have pathologic results.

Table 1: Participant Characteristics at Imaging

Characteristic	Healthy Control Participants ($n = 15$)	Participants with NSIP ($n = 36$)	P Value
Sex			
M	13	9	NA
F	2	27	NA
Mean age (y)*	39 ± 18	57 ± 11	<.001
Lung function at imaging			
FVC%†	92.0 (87.3, 105.3)	63.5 (52.0, 75.3)	<.001
DLco%†	85.5 (80.3, 90.8)	53.5 (40.8, 75.0)	<.001
ILD-GAP score			
<0	NA	7 (19)	NA
0–1	NA	22 (61)	NA
>1	NA	7 (19)	NA
Pulmonary artery diameter (cm)†	NA	3.0 (2.8, 3.3)	NA
Therapy at imaging			
None	NA	6 (17)	NA
Prednisone alone	NA	4 (11)	NA
Advanced therapy with or without prednisone	NA	25 (71)	NA

Note.—Except where indicated, data are numbers of participants, with percentages in parentheses. Healthy control participants were not required to undergo CT and thus do not have pulmonary artery measurements. DLco% = percentage of predicted diffusing capacity of the lung for carbon monoxide, FVC% = percentage of predicted forced vital capacity, ILD-GAP = Interstitial Lung Disease–Gender-Age-Physiology, NA = not applicable, NSIP = nonspecific interstitial pneumonia.

* Numbers are means ± standard deviations.

† Numbers are medians. The first number in parentheses is the first quartile, and the second number in parentheses is the third quartile.

where the dose equivalent is the hypothetical volume of pure, 100% hyperpolarized ^{129}Xe that would produce the same net magnetization as the dose being sampled) and a larger dose for the imaging scan (target dose equivalent ≥150 mL; actual dose: mean, 175.6 mL ± 31.9). These doses required xenon volumes (86% enriched in ^{129}Xe), which ranged 210–720 mL depending on the type of acquisition, and which were expanded with a nonpolarized ^{129}Xe blend to achieve a net 1-L dose delivery bag volume. The bag was then inhaled from functional residual capacity. Supplementary oxygen was administered as needed by means of a nasal cannula that was removed two breaths (approximately 10–12 seconds) before ^{129}Xe inhalation. Heart rate and oxygen saturation were continuously monitored with an MRI-compatible monitoring system (Model 7500, Nonin).

The combined calibration and spectroscopy scan was performed during a 16-second breath hold and acquired 600 ^{129}Xe free-induction decays at 20-msec intervals (echo time, 0.45 msec; target flip angle, 20°; dwell time, 37 μsec; 512 points) (24). Three-dimensional images were obtained during a 15-second breath hold using an interleaved radial acquisition of gas- and dissolved-phase (ie, barrier uptake and RBC) signals. Dissolved-phase images were obtained with an effective repetition time of 15 msec and flip angle of 20° and an echo time that allowed the dissolved-phase compartments to be decomposed using the one-point Dixon method (25). This process generated three-dimensional images of the gas, barrier uptake, and RBC components with a nominal isotropic resolution of 6.3 mm.

Image Processing and Analysis
Quantification of ^{129}Xe MRI scans was performed according to previously published methods (26). Gas phase ^{129}Xe MRI scans were rendered into quantitative maps by normalizing to the top intensity percentile and assigning each voxel into one of six classification "bins" using pre-existing thresholds previously derived from a healthy reference population (26).

Barrier uptake and RBC images were divided by gas-phase intensities on a voxel-by-voxel basis to create maps relative to the gas signal, which were also cast into bins (six for RBC and eight for barrier uptake due to its greater dynamic range) as described previously (26). All measurements of barrier uptake and RBC transfer were calculated relative to the gas phase signal. Ventilation was quantified by using the ventilation defect percentage (VDP), corresponding to the signal at least 2 standard deviations below the healthy reference mean (ie, the lowest bin). Barrier uptake was quantified by using the high barrier uptake percentage, corresponding to the signal at least 2 standard deviations above the healthy reference mean (ie, the three highest bins). RBC transfer was quantified using the RBC defect percentage (RDP), corresponding to the signal at least 2 standard deviations below the reference mean (ie, the lowest bin) (26,27).

Healthy 95th-Percentile Calculation
For each of these metrics—VDP, high barrier uptake percentage, and RDP—we calculated the observed 95th-percentile value
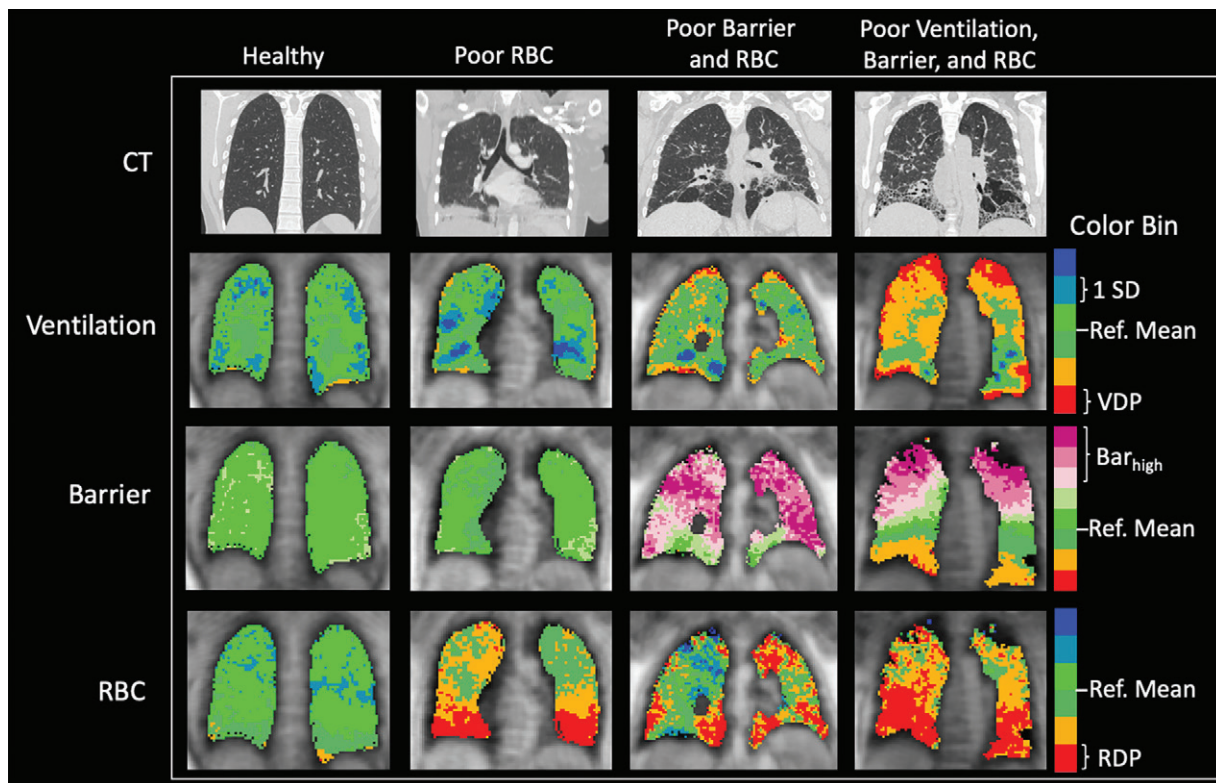
Figure 2: Representative CT scans, xenon 129 (¹²⁹Xe) MRI ventilation scans, barrier scans, and red blood cell (RBC) scans in healthy control participant and three participants with nonspecific interstitial pneumonia (NSIP) and range of findings (from left to right: man, age 24 years; woman, age 46 years; woman, age 55 years; and woman, age 57 years). Orange and red indicate reduced signal in ventilation and RBC components, indicating abnormalities. Purple indicates increased signal in barrier component, possibly indicating thickened barrier and/or fibrosis. The first and third scans in participants with NSIP (second and fourth columns in figure) show common pattern of basilar-predominant RBC transfer defects. Note that although these RBC transfer defects are ubiquitous features in participants with NSIP, some participants with NSIP have preserved, normal-looking barrier uptake and/or ventilation. Regional correspondence is visible between CT and ¹²⁹Xe MRI abnormalities. Notably, regions of high barrier measured using ¹²⁹Xe MRI are also associated with normal CT findings, suggesting early-stage microstructural disease activity not yet visible on CT scan. Bar$_{high}$ = high barrier percentage, Ref. = reference, RDP = red blood cell defect percentage, SD = standard deviation, VDP = ventilation defect percentage.

in healthy control participants (H95%) as 2 standard deviations above the corresponding mean value of that metric in our healthy control population.

Spectroscopy Processing and Analysis

Dynamically acquired free-induction decays were fit to three peaks (ie, gas, barrier uptake, and RBC transfer) in the time domain with each peak described by an amplitude, chemical shift, phase, and either one (gas and RBC) or two (barrier uptake) full widths at half maximum (24). Spectroscopy indexes included the RBC-to-barrier ratio, RBC static chemical shift, and cardiogenic oscillations of the RBC signal amplitude and chemical shift, which were quantified with peak-to-peak value relative to the mean (24). For participants who underwent dynamic spectroscopy scanning twice in the same imaging session as part of a concurrent study to assess repeatability of spectroscopy measurements, the mean of the measurements was used for analysis.

Statistical Analysis

Differences between the healthy group and participants with NSIP were assessed using the Wilcoxon rank-sum test. To account for multiple comparisons when testing our primary

hypothesis, we applied a Bonferroni correction with m = 7 corresponding to the three imaging-based and four spectroscopy-based tests, yielding a significance threshold of $P <$ .05/7 = .0071. All other rank-sum tests were evaluated with a statistical significance of $P <$ .05. Correlations with clinical metrics were assessed using the Spearman correlation with a statistical significance of $P <$ .05. Statistical analysis was performed with R software (version 3.6.0, R Foundation for Statistical Computing) (28).

Results

Participant Characteristics

Thirty-six participants with NSIP (mean age, 57 years ± 11; 27 women) and 15 healthy control participants (mean age, 39 years ± 18; two women) were enrolled between November 2017 and February 2020 (Fig 1). Surgical lung biopsies obtained from 13 participants had a confirmed NSIP pattern identified at pathologic examination. Six participants had inconclusive pathologic findings, and the remaining 17 did not undergo a biopsy. The CT scans used for screening occurred at a mean of 597 days ± 529 before the study visit. Basic demographic, clinical, and treatment character-

istics of our population are shown in Table 1. Participants with NSIP had a lower percentage of predicted forced vital capacity and percentage of predicted diffusing capacity of the lung for carbon monoxide versus healthy control participants (median, 63.5% [first quartile, 52.0%; third quartile, 75.3%] vs 92% [first quartile, 87.3%; third quartile, 105.3%] and median, 53.5% [first quartile, 40.8%; third quartile, 75.0%] vs 85.5% [first quartile, 80.3%; third quartile, 90.3%], respectively; $P < .001$ for both). Seven of the

36 participants with NSIP (19%) had an ILD–Gender-Age-Physiology score lower than 0, 22 (61%) had a score of 0 or 1, and seven (19%) had a score higher than 1. Participants with NSIP had a median pulmonary artery diameter of 3.0 cm (first quartile, 2.8 cm; third quartile, 3.3 cm) measured using CT and a resting peripheral capillary oxygen saturation of 98% (first quartile, 96%; third quartile, 99%), with four participants requiring supplementary oxygen at rates of 2–6 L/min.

Of the 29 participants receiving treatment for NSIP at imaging, four (14%) were receiving prednisone alone, and the remaining 25 (86%) were receiving a more advanced therapy with or without prednisone, including mycophenolate, rituximab, azathioprine, pirfenidone, and/or mycophenolic acid. Medical history was unavailable for one participant who received care outside our health system.

Representative ^{129}Xe MRI Findings

Figure 2 shows representative CT and ^{129}Xe MRI scans from a healthy control participant and three participants with NSIP. Typical spectroscopic findings from a participant with NSIP and a healthy control participant are shown in Figure 3. Imaging and spectroscopy metrics for participants with NSIP and healthy control participants are presented in Table 2. The mean VDP in the healthy control participants was 5.5% ± 4.2, resulting in a H95% of 13.8%. The high barrier uptake percentage was 2.8% ± 5.2, resulting in a H95% of 13.1%, and the RDP was 4.4% ± 4.2, resulting in a H95% of 12.8%. The healthy control participants and participants with NSIP were directly compared using box plots for each metric (Fig 4) and the Wilcoxon rank-sum test. The VDP did not differ between the participants with NSIP and the healthy control participants (median, 4.4% [first quartile,
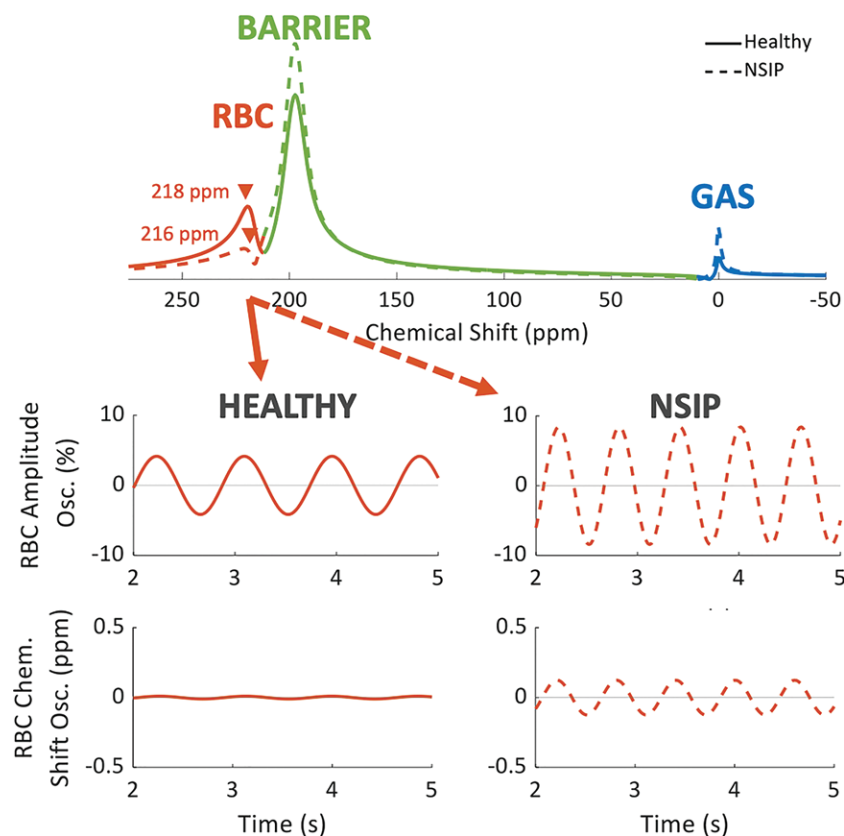

Figure 3: Graphs of xenon 129 MR spectroscopy results in participant with nonspecific interstitial pneumonia (NSIP) (woman, age 67 years; dashed orange line) and healthy control participant (man, age 63 years; solid orange line). Difference in red blood cell (RBC) and barrier peaks leading to reduced RBC-to-barrier ratio is clearly visible in participant with NSIP. Also note reduced chemical (Chem.) shift in RBC peak and increased RBC amplitude and chemical shift oscillations (Osc.) associated with cardiac cycle in participant with NSIP.

Table 2: Xenon 129 MRI and Spectroscopy Metrics for Healthy Control Participants and Participants with NSIP

| Metric	Healthy Control Participants ($n = 15$)	Participants with NSIP ($n = 36$)	P Value
VDP (%)	6.0 (2.8, 6.9)	4.4 (1.5, 8.7)	.91
High barrier percentage (%)	0.53 (0.33, 2.9)	6.2 (1.8, 23.9)	.003
RDP (%)	2.8 (2.3, 4.9)	20.6 (11.6, 27.8)	<.001
RBC-to-barrier ratio	0.57 (0.52, 0.67)	0.24 (0.19, 0.31)	<.001
RBC static chemical shift (ppm)	218.2 (217.9, 218.6)	217.5 (217.0, 218.0)	.001
RBC amplitude oscillations (%)	8.1 (7.6, 9.4)	15.4 (12.6, 19.3)	<.001
RBC chemical shift oscillations (ppm)	0.04 (0.04, 0.06)	0.11 (0.06, 0.14)	<.001

Note.—Data are medians. The first number in parentheses is the first quartile, and the second number in parentheses is the third quartile. Two healthy control participants and four participants with nonspecific interstitial pneumonia (NSIP) did not have usable spectroscopy results and are omitted from spectroscopic measurements. RBC = red blood cell, RDP = red blood cell defect percentage, VDP = ventilation defect percentage.
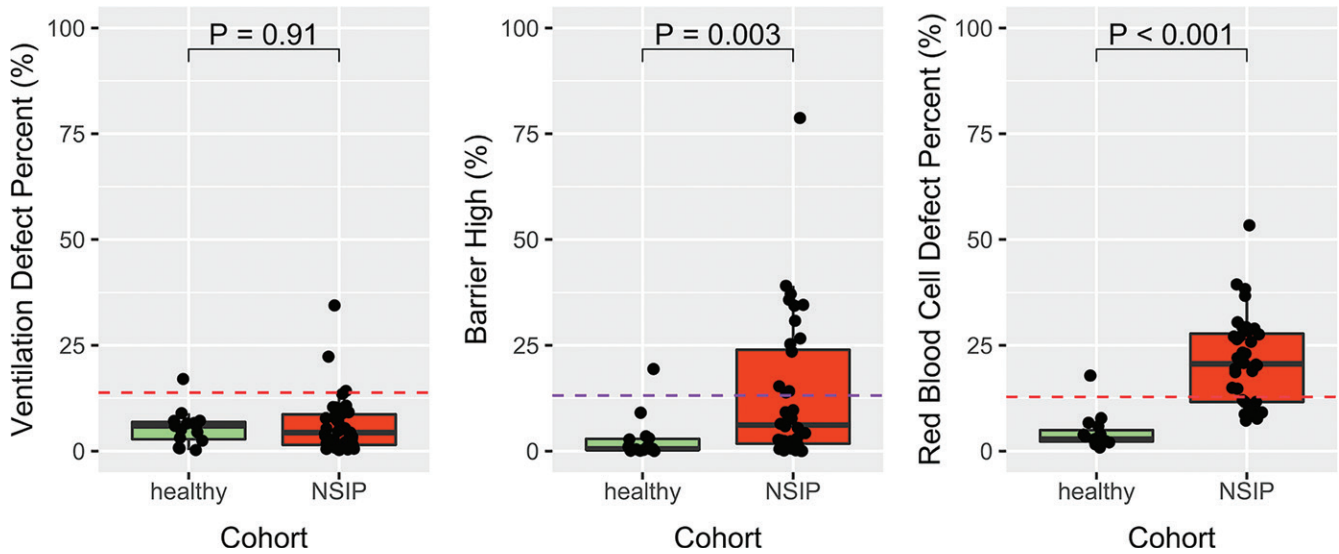
Figure 4: Box plots show ventilation defect percentage, high barrier uptake percentage, and red blood cell defect percentage in healthy control participants and participants with nonspecific interstitial pneumonia (NSIP). Horizontal dashed lines indicate observed 95th-percentile values in healthy control participants as determined using mean + 2 standard deviations in healthy control participants. Each black dot is an individual study participant. Horizontal solid lines are first quartile, median, and third quartile. Both high barrier uptake percentage and red blood cell defect percentage were higher in participants with NSIP than in healthy control participants (median, 6.2% [first quartile, 1.8%; third quartile, 23.9%] vs 0.53% [first quartile, 0.33%; third quartile, 2.9%]; $P = .003$ and median, 20.6% [first quartile, 11.6%; third quartile, 27.8%] vs 2.8% [first quartile, 2.3%; third quartile, 4.9%]; $P < .001$, respectively). Ventilation defect percentage did not differ between the two groups (median, 4.4% [first quartile, 1.5%; third quartile, 8.7%] vs 6.0% [first quartile, 2.8%; third quartile, 6.9%]; $P = .91$).
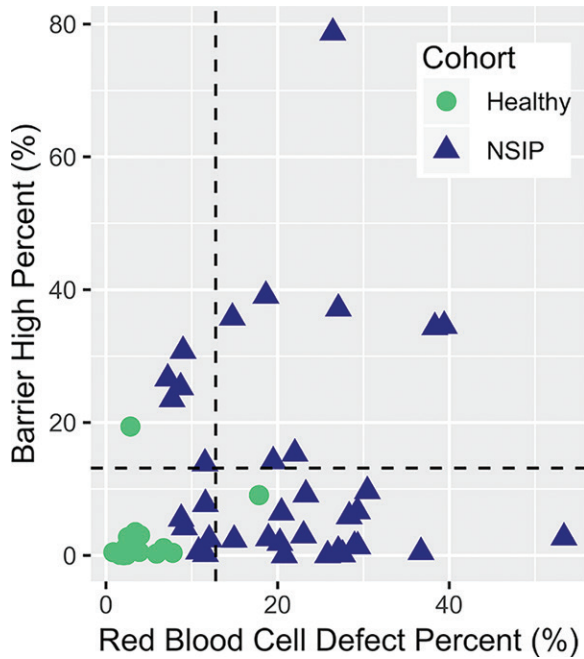
Figure 5: Scatterplot shows distribution of high barrier uptake percentage and red blood cell defect percentage in participants with nonspecific interstitial pneumonia (NSIP) (triangles) and healthy control participants (circles). High barrier uptake percentage for the observed 95th percentile in healthy control participants (12.7%) and red blood cell defect percentage for the observed 95th percentile in healthy control participants (12.8%) are indicated by dashed lines.
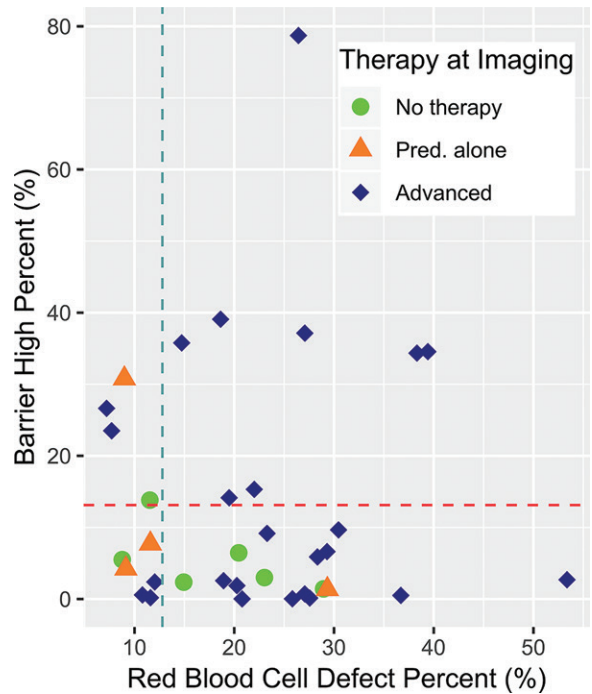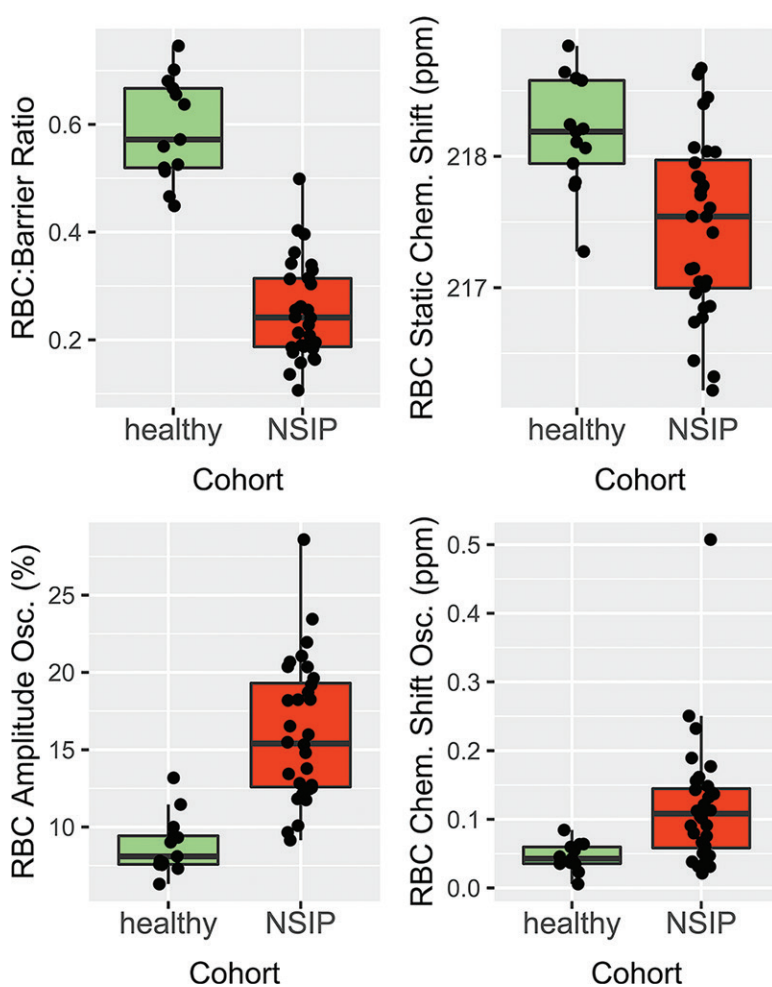

Figure 6: Scatterplot shows treatment at imaging in 35 participants with nonspecific interstitial pneumonia. Six participants (17%) were receiving no treatment (circles), four participants (11%) were receiving prednisone (Pred.) alone (triangles), and the remaining 25 (71%) were receiving more advanced therapy with or without prednisone (diamonds). The high barrier percentage for the observed 95th percentile in healthy control participants (13.1%) and red blood cell defect percentage for observed 95th percentile in healthy control participants (12.8%) are indicated by dashed lines. Note that all participants who were not receiving therapy had high barrier uptake percentage at or below the observed 95th percentile in healthy control participants.

1.5%; third quartile, 8.7%] vs 6.0% [first quartile, 2.8%; third quartile, 6.9%]; P = .91), although the population with NSIP had a wide distribution around the median, suggesting variability in individual participants. Both high barrier uptake percentage and RDP were higher in the participants with NSIP compared with the healthy control participants (median, 6.2% [first quartile, 1.8%; third quartile, 23.9%] vs 0.53% [first quartile, 0.33%; third quartile, 2.9%]; P = .003 and median, 20.6% [first quartile, 11.6%; third quartile, 27.8%]% vs 2.8% [first quartile, 2.3%; third quartile, 4.9%]; $P <$ .001 respectively).

The scatterplot in Figure 5 illustrates the distribution of high barrier uptake percentage and RDP in the healthy control participants compared with that in participants with NSIP. In the participants with NSIP, high barrier uptake percentage exceeded H95% in 13 of 36 participants (36%), whereas RDP exceeded H95% in 25 of 36 participants (69%); both metrics exceeded their respective H95% in eight of 36 participants (22%). Conversely, for healthy control participants, all but two of 15 (13%) were below both H95% values, and none exceeded both H95% values.

In the participants with NSIP, treatment status is shown relative to high barrier uptake percentage and RDP in Figure 6. All eight participants with both high barrier uptake percentage and RDP above their corresponding H95% (upper right quadrant) were receiving an advanced therapy (ie, more than prednisone alone). Among the participants with one or both metrics below the corresponding H95%, this proportion was reduced to 17 of 27 participants (63%).

Spectroscopy Findings

RBC amplitude oscillations and chemical shift in the healthy control participants and participants with NSIP are shown in Figure 7. An illustration of proposed physiology underlying RBC oscillation measurements is available in Figure E1 (online). Two healthy control participants and four participants with NSIP did not have usable spectroscopy findings and were omitted. Eight healthy control participants and 25 participants with NSIP underwent spectroscopy scanning twice, which were averaged. The remaining five healthy control participants and seven participants with NSIP underwent spectroscopy scanning once. The RBC-to-barrier ratio was lower in participants with NSIP than in healthy control participants (median, 0.24 [first quartile, 0.19; third quartile, 0.31] vs 0.57 [first quartile, 0.52; third quartile, 0.67]; $P <$ .001) as was the RBC static chemical shift (median, 217.5 ppm [first quartile, 217.0 ppm; third quartile, 218.0 ppm] vs 218.2 ppm [first quartile, 217.9 ppm; third quartile, 218.6 ppm]; $P <$ .001). RBC amplitude oscillations were higher in participants with NSIP than in healthy control participants (median, 15.4% [first quartile, 12.6%; third quartile, 19.3%] vs 8.1% [first quartile, 7.6%; third quartile, 9.4%]; P = .001), as were chemical shift oscillations (median, 0.11 ppm [first quartile, 0.06 ppm; third quartile, 0.14 ppm] vs 0.04 ppm [first quartile, 0.04 ppm; third quartile, 0.06 ppm]; $P <$ .001).

Figure 7: Top row: Box plots show that static xenon 129 MR spectroscopy measurements of red blood cell (RBC)–to-barrier ratio and RBC static chemical (Chem.) shift are lower in participants with nonspecific interstitial pneumonia (NSIP) than in healthy control participants ($P <$ .001 and P = .001 respectively). Bottom row: Box plots of dynamic spectroscopy measurements show that RBC amplitude oscillations (Osc.) and RBC chemical shift oscillations are higher in participants with NSIP than in healthy control participants ($P <$ .001 for both). Each black dot is an individual study participant. Horizontal solid lines are the first quartile, median, and third quartile.

Correlations with Pulmonary Function Tests

Correlations between [129]Xe MRI and spectroscopy measurements and percentage of predicted diffusing capacity of the lung for carbon monoxide and percentage of predicted forced vital capacity are shown in Tables 3 and 4. An increased high barrier uptake percentage was associated with reduced percentage of predicted forced vital capacity (r = −0.37, P = .03). The RBC-to-barrier ratio was associated with increased percentage of predicted diffusing capacity of the lung for carbon monoxide (r = 0.49, P = .005). RDP and RBC chemical shift were associated with reduced percentage of predicted diffusing capacity of the lung for carbon monoxide (r = −0.47, $P <$ .01 and r = −0.36, P = .043 respectively).

Discussion

Participants with nonspecific interstitial pneumonia (NSIP) had no difference in ventilation com-

Table 3: Spearman Rho Correlations of DLco% with Xenon 129 MRI and Spectroscopy Measurements

Metric	Healthy Control Participants (*n* = 15)	Participants with NSIP (*n* = 35)
VDP (%)	0.19 (.51)	−0.09 (.62)
High barrier uptake percentage (%)	−0.14 (.63)	−0.20 (.25)
RDP (%)	−0.01 (.97)	−0.47 (.004)
RBC-to-barrier ratio	0.01 (.96)	0.49 (.005)
RBC static chemical shift (ppm)	−0.04 (.89)	0.31 (.09)
RBC amplitude oscillations (%)	0.22 (.47)	−0.04 (.83)
RBC chemical shift oscillations (ppm)	−0.08 (.80)	−0.36 (.043)

Note.—Numbers in parentheses are *P* values. DLco% = percentage of predicted diffusing capacity of the lung for carbon monoxide, NSIP = nonspecific interstitial pneumonia, RBC = red blood cell, RDP = red blood cell defect percentage, VDP = ventilation defect percentage.

Table 4: Spearman Rho Correlations of FVC% with Xenon 129 MRI and Spectroscopy Measurements

Metric	Healthy Control Participants (*n* = 15)	Participants with NSIP (*n* = 35)
VDP (%)	0.01 (.98)	−0.02 (.92)
High barrier uptake percentage (%)	−0.05 (.86)	−0.37 (.03)
RDP (%)	0.05 (.88)	−0.08 (.63)
RBC-to-barrier ratio	0.08 (.79)	0.06 (.75)
RBC static chemical shift (ppm)	0.03 (.93)	0.21 (.25)
RBC amplitude oscillations (%)	0.32 (.28)	0.02 (.93)
RBC chemical shift oscillations (ppm)	0.29 (.33)	−0.03 (.86)

Note.—Numbers in parentheses are *P* values. FVC% = percentage of predicted forced vital capacity, NSIP = nonspecific interstitial pneumonia, RBC = red blood cell, RDP = red blood cell defect percentage, VDP = ventilation defect percentage.

pared with healthy control participants observed with ^{129}Xe gas-exchange MRI, but they had a higher barrier uptake and reduced red blood cell (RBC) transfer. Spectroscopy showed that participants with NSIP had a reduced RBC-to-barrier ratio, reduced RBC chemical shift, increased RBC amplitude oscillations, and increased RBC chemical shift oscillations. Percentage of predicted diffusing capacity of the lung for carbon monoxide in our population with NSIP was positively correlated with RBC-to-barrier ratio and negatively correlated with RDP and RBC chemical shift. Percentage of predicted forced vital capacity was negatively correlated with high barrier uptake percentage.

We observed consistent RBC transfer impairment in participants with NSIP, often exhibiting a basilar predominant pattern. More than two-thirds of the participants with NSIP had a RDP above the corresponding H95% value, and it was above the third quartile of healthy control participants in every participant with NSIP. Conversely, although the high barrier uptake percentage was significantly increased relative to the healthy control participants, it only exceeded the corresponding H95% value in 13 of 36 NSIP participants (36%). One possible explanation lies in the fact that the majority of participants were receiving a range of therapies known to effectively treat NSIP, as preliminary studies in IPF have suggested that effective therapy reduces barrier uptake while minimally affecting RBC transfer (29). Therefore, we speculate that the relatively normalized barrier in many participants with NSIP may reflect slowed disease progression because of effective therapy, whereas the persistently increased RDP reflects lasting and irreversible damage caused by fibrosis. Similar patterns of increased ^{129}Xe barrier tissue uptake and subsequent reduction in transfer to RBCs have been observed in IPF (17). Interestingly, although the overall VDP distribution in the population with NSIP was no different from the healthy control participants, two of the three participants with NSIP with VDP over the corresponding H95% value had a very high VDP (34.4% and 22.3%), suggesting the possibility of airway obstruction in a subset of patients with NSIP.

Static and dynamic spectroscopy measurements further suggest that underlying alterations in gas exchange are similar between patients with NSIP and those with IPF. Most fundamentally, the reduction in RBC-to-barrier ratio reflects the concomitant increase in barrier uptake and a decrease in RBC transfer seen when measured using ^{129}Xe MRI in our study. This measurement also appears to be more sensitive to disease progression in patients with IPF than conventional clinical metrics (18). This is also consistent with the ubiquitous RBC transfer defects observed on images in our participants with NSIP and the significantly reduced percentage of predicted diffusing capacity of the lung for carbon monoxide. The reduced RBC chemical shift and its oscillatory behavior suggests lower and more delayed oxygenation in the pulmonary capillary bed, as RBC chemical shift is known to be dependent on oxygen saturation level (30).

Increased RBC amplitude oscillations have previously been observed in patients with IPF (17,20) and were hypothesized to be the result of increased impedance to blood flow because of a partially destroyed capillary bed (17). In this scenario, a preserved cardiac stroke volume is forced through a reduced amount of pulmonary vasculature, thus provoking larger signal oscillations (16). This observation in conjunction with RBC defects on images suggests that a similar phenomenon may take place in patients with NSIP. Further, the increased RBC chemical shift oscillations seen in patients with NSIP were also observed in patients with IPF but not in those with other cardiovascular diseases. The clinical significance of this finding is not yet clear but was hypothesized to be related to large excursions in blood oxygenation as capillary blood volume is replenished in a thickened or otherwise diffusively impaired interstitium during the cardiac cycle (16). That this finding is also demonstrated in patients with NSIP further suggests that it is a feature common to ILD-related fibrosis.

Our study had limitations. First among these was the confounding effect of therapy. Given the availability of efficacious treatment for patients with NSIP, it was not possible to recruit

a treatment-naive population. Although participants with NSIP who were above the H95% for both the high barrier uptake percentage and RDP were uniformly receiving advanced therapy, some participants below one or both of these H95% values were also undergoing advanced therapy. Although this is consistent with the hypothesis that effective treatment may reduce abnormalities detected using [129]Xe MRI, we could not assess any causal relationship between therapy and [129]Xe MRI findings. Second, our group of healthy control participants was younger than our population with NSIP and was predominantly composed of men. Because more women show NSIP patterns and are known to have an altered immune response, and age is a factor in lung function decline, we acknowledge that an age- and sex-matched control population would result in a more specific comparison. However, this does not affect the variation in measurements between individual ILD patients. Further, the observed differences in gas-exchange function between healthy control participants and participants with NSIP are far starker in pattern and degree than would be expected of ordinary age and/or sex differences. Third, although preliminary studies have shown that dissolved-phase MRI has good repeatability in a cohort of healthy patients (31), neither the repeatability nor the minimal clinically important difference of these measurements in fibrotic lung disease have been characterized. Fourth, the average time between the screening CT examination and the [129]Xe MRI examination was almost 2 years. To ensure the availability of contemporaneous clinical findings, it would be preferable to recruit patients immediately after they undergo clinical CT and are examined by a pulmonologist. Finally, our study did not attempt to establish correlations between [129]Xe MRI and other aspects of a multi-disciplinary ILD diagnosis such as pathologic findings and CT. Nonetheless, our results are a necessary first step for characterizing the presentation of patients with NSIP assessed with [129]Xe gas-exchange MRI and for determining possible markers of therapy response in patients with ILD in a broader way.

In conclusion, these preliminary results suggest that hyperpolarized xenon-129 ([129]Xe) MRI and spectroscopy may illuminate the fundamental abnormalities and regional severity of gas exchange that occur in patients with nonspecific interstitial pneumonia and in those with potentially other non–idiopathic pulmonary fibrosis interstitial lung diseases. Future studies focused on [129]Xe MRI characteristics early in the disease course and in response to therapies will advance this work and will further explore its potential clinical impact. This new modality may serve to identify "treatable traits," (32) monitor therapy response, and personalize treatment in this disorder.

References

1. Travis WD, Hunninghake G, King TE Jr, et al. Idiopathic nonspecific interstitial pneumonia: report of an American Thoracic Society project. Am J Respir Crit Care Med 2008;177(12):1338–1347.
2. Bedoya A, Pleasants RA, Boggan JC, et al. Interstitial lung disease in a veterans affairs regional network; a retrospective cohort study. PLoS One 2021;16(3):e0247316.
3. Sumikawa H, Johkoh T, Fujimoto K, et al. Pathologically proved nonspecific interstitial pneumonia: CT pattern analysis as compared with usual interstitial pneumonia CT pattern. Radiology 2014;272(2):549–556.
4. Ebner L, Christodoulidis S, Stathopoulou T, et al. Meta-analysis of the radiological and clinical features of Usual Interstitial Pneumonia (UIP) and Nonspecific Interstitial Pneumonia (NSIP). PLoS One 2020;15(1):e0226084.
5. Nunes H, Schubel K, Piver D, et al. Nonspecific interstitial pneumonia: survival is influenced by the underlying cause. Eur Respir J 2015;45(3):746–755.
6. Wong AW, Ryerson CJ, Guler SA. Progression of fibrosing interstitial lung disease. Respir Res 2020;21(1):32.
7. George PM, Spagnolo P, Kreuter M, et al. Progressive fibrosing interstitial lung disease: clinical uncertainties, consensus recommendations, and research priorities. Lancet Respir Med 2020;8(9):925–934.
8. Richeldi L, du Bois RM, Raghu G, et al. Efficacy and safety of nintedanib in idiopathic pulmonary fibrosis. N Engl J Med 2014;370(22):2071–2082.
9. King TE Jr, Bradford WZ, Castro-Bernardini S, et al. A phase 3 trial of pirfenidone in patients with idiopathic pulmonary fibrosis. N Engl J Med 2014;370(22):2083–2092.
10. Flaherty KR, Wells AU, Cottin V, et al. Nintedanib in Progressive Fibrosing Interstitial Lung Diseases. N Engl J Med 2019;381(18):1718–1727.
11. Distler O, Highland KB, Gahlemann M, et al. Nintedanib for Systemic Sclerosis-Associated Interstitial Lung Disease. N Engl J Med 2019;380(26):2518–2528.
12. Moua T, Zamora Martinez AC, Baqir M, Vassallo R, Limper AH, Ryu JH. Predictors of diagnosis and survival in idiopathic pulmonary fibrosis and connective tissue disease-related usual interstitial pneumonia. Respir Res 2014;15(1):154.
13. Roos JE, McAdams HP, Kaushik SS, Driehuys B. Hyperpolarized gas MR imaging: technique and applications. Magn Reson Imaging Clin N Am 2015;23(2):217–229.
14. Kaushik SS, Freeman MS, Yoon SW, et al. Measuring diffusion limitation with a perfusion-limited gas--hyperpolarized 129Xe gas-transfer spectroscopy in patients with idiopathic pulmonary fibrosis. J Appl Physiol (1985) 2014;117(6):577–585.
15. Freeman MS, Cleveland ZI, Qi Y, Driehuys B. Enabling hyperpolarized (129) Xe MR spectroscopy and imaging of pulmonary gas transfer to the red blood cells in transgenic mice expressing human hemoglobin. Magn Reson Med 2013;70(5):1192–1199.
16. Wang Z, Bier EA, Swaminathan A, et al. Diverse cardiopulmonary diseases are associated with distinct xenon magnetic resonance imaging signatures. Eur Respir J 2019;54(6):1900831.
17. Wang JM, Robertson SH, Wang Z, et al. Using hyperpolarized [129]Xe MRI to quantify regional gas transfer in idiopathic pulmonary fibrosis. Thorax 2018;73(1):21–28.
18. Weatherley ND, Stewart NJ, Chan HF, et al. Hyperpolarised xenon magnetic resonance spectroscopy for the longitudinal assessment of changes in gas diffusion in IPF. Thorax 2019;74(5):500–502.

19. Rankine LJ, Wang Z, Wang JM, et al. ^{129}Xenon Gas Exchange Magnetic Resonance Imaging as a Potential Prognostic Marker for Progression of Idiopathic Pulmonary Fibrosis. Ann Am Thorac Soc 2020;17(1):121–125.

20. Niedbalski PJ, Bier EA, Wang Z, Willmering MM, Driehuys B, Cleveland ZI. Mapping cardiopulmonary dynamics within the microvasculature of the lungs using dissolved ^{129}Xe MRI. J Appl Physiol (1985) 2020;129(2):218–229.

21. Raghu G, Remy-Jardin M, Myers JL, et al. Diagnosis of Idiopathic Pulmonary Fibrosis. An Official ATS/ERS/JRS/ALAT Clinical Practice Guideline. Am J Respir Crit Care Med 2018;198(5):e44–e68.

22. Ryerson CJ, Vittinghoff E, Ley B, et al. Predicting survival across chronic interstitial lung disease: the ILD-GAP model. Chest 2014;145(4):723–728.

23. He M, Robertson SH, Kaushik SS, et al. Dose and pulse sequence considerations for hyperpolarized (129)Xe ventilation MRI. Magn Reson Imaging 2015;33(7):877–885.

24. Bier EA, Robertson SH, Schrank GM, et al. A protocol for quantifying cardiogenic oscillations in dynamic ^{129}Xe gas exchange spectroscopy: The effects of idiopathic pulmonary fibrosis. NMR Biomed 2019;32(1):e4029.

25. Kaushik SS, Robertson SH, Freeman MS, et al. Single-breath clinical imaging of hyperpolarized (129)Xe in the airspaces, barrier, and red blood cells using an interleaved 3D radial 1-point Dixon acquisition. Magn Reson Med 2016;75(4):1434–1443.

26. Wang Z, Robertson SH, Wang J, et al. Quantitative analysis of hyperpolarized ^{129}Xe gas transfer MRI. Med Phys 2017;44(6):2415–2428.

27. Kirby M, Heydarian M, Svenningsen S, et al. Hyperpolarized 3He magnetic resonance functional imaging semiautomated segmentation. Acad Radiol 2012;19(2):141–152https://doi.org/10.1016/j.acra.2011.10.007.

28. R Core Team. R: a language and environment for statistical computing [online]. Vienna, Austria: R Foundation for Statistical Computing, 2018. https://www.r-project.org. Accessed June 5, 2019.

29. Mummy D, Rankine L, Wang Z, et al. Hyperpolarized 129Xe Magnetic Resonance Imaging Is Sensitive to Therapy Response in Idiopathic Pulmonary Fibrosis. In: D110 New Insights from Advanced Imaging. New York, NY: American Thoracic Society, 2020; A7902.

30. Norquay G, Leung G, Stewart NJ, Wolber J, Wild JM. ^{129}Xe chemical shift in human blood and pulmonary blood oxygenation measurement in humans using hyperpolarized ^{129}Xe NMR. Magn Reson Med 2017;77(4):1399–1408.

31. Hahn AD, Kammerman J, Evans M, et al. Repeatability of regional pulmonary functional metrics of Hyperpolarized ^{129}Xe dissolved-phase MRI. J Magn Reson Imaging 2019;50(4):1182–1190.

32. Agusti A, Bel E, Thomas M, et al. Treatable traits: toward precision medicine of chronic airway diseases. Eur Respir J 2016;47(2):410–419.